*R*esearch in
*A*stronomy and
*A*strophysics

Quasar SDSS J142507.32+323137.4: dual AGNs? *

Zhi-Xin Peng[1,2], Yan-Mei Chen[1,2], Qiu-Sheng Gu[1,2] and Chen Hu[3]

[1] Department of Astronomy, Nanjing University, Nanjing 210093, China; *zxpeng@nju.edu.cn*
[2] Key Laboratory of Modern Astronomy and Astrophysics (Nanjing University), Ministry of Education, Nanjing 210093, China
[3] Key Laboratory for Particle Astrophysics, Institute of High Energy Physics, Chinese Academy of Sciences, Beijing 100049, China

Abstract We analyze the optical spectrum of type 1 QSO SDSS J1425+3231. This object is interesting since its narrow emission lines, such as [O III]$\lambda\lambda$4959, 5007, are double-peaked, and the line structure can be modeled well by three Gaussian components: two components for the two peaks (we refer to the peaks at low/high redshift as "the blue/red component") and another one for the line wing which has the same line center as that of the blue component, but is ~ 3 times broader. The separation between the blue and red components is $\sim 500 \, \mathrm{km \, s^{-1}}$ with the blue component being ~ 2 times broader than the red one. The Hβ emission can be separated into four components: two for the double-peaked narrow line and two for the broad line which comes from the broad line regions. The black hole mass estimated from the broad Hβ emission line using the typical reverberation mapping relation is $0.85 \times 10^8 \, M_\odot$, which is consistent with that derived from parameters of [O III]λ 5007 of the blue component. We suggest that this QSO might be a dual AGN system; the broad Hβ emission line is mainly contributed by the primary black hole (traced by the blue component) while the broad Hβ component of the secondary black hole (traced by the red component) is hard to be separated out considering a resolution of $\sim 2\,000$ for SDSS spectra or it may be totally obscured by the dusty torus.

Key words: galaxies: active — galaxies: individual (SDSS J142507.32+323137.4) — quasars: emission lines

1 INTRODUCTION

Early in the 1980s, the double-peaked narrow emission lines in active galactic nuclei (AGNs) have been reported by Heckman et al. (1981, 1984), and they suggested biconic outflows as an origin of double peaked AGNs. Greene & Ho (2005) pointed out that about 1% of local AGNs have double-peaked narrow emission lines. Since narrow emission lines are generally believed to be produced by clouds in the narrow line regions (NLRs), they suggested the simplest explanation to be that $\sim$1% of AGNs have disk-like NLRs. A double-peaked AGN fraction of $\sim$1% has also been found by Zhou et al. (2004) and Wang et al. (2009). In particular, the flux ratios of the two peaks of [O III]λ 5007 are statistically anti-correlated with the ratios between their red and blue shifts relative to the host

galaxies. This phenomenon could be understood as a natural result of Kepler rotation of dual AGNs, leading to another possible explanation of double-peaked narrow emission lines (Wang et al. 2009).

In the last two years, more and more attention has been paid to the study of dual AGNs (e.g. Comerford et al. 2009a,b; Dotti et al. 2009; Boroson & Lauer 2009; Xu & Komossa 2009; Liu et al. 2010) since on the one hand, they are unavoidable results of the hierarchical cosmology model which has gained great success; on the other hand, with the launch of X-ray and infrared space astronomical facilities (Chandra, Spitzer, and Herschel Space telescopes), it is now possible for us to resolve the dual AGNs which have kpc-scale separations. Observational evidence for dual AGNs includes: spatially resolved systems in which both supermassive black holes (SMBHs) can be identified directly and spatially unresolved systems in which the dual AGN model can explain various phenomena (see Komossa 2006 for a detailed review). Most recently, Colpi & Dotti (2009) further summarized the observations and numerical simulations of dual and binary black holes. So far, a few unambiguous cases have been found, such as NGC 6240 (Komossa et al. 2003), J0402+379 (Rodriguez et al. 2006, 2009; Morganti et al. 2009), EGSD2 J142033+525917 (Gerke et al. 2007), EGSD2 J141550+520929 (Comerford et al. 2009a), COSMOS J100043+020637 (Comerford et al. 2009b), and four other dual AGNs (see Liu et al. 2010). There are other interesting sources, which need more verification by future observations. Zhou et al. (2004) connected both SDSS and VLBA data, suggesting SDSS J1048+0055 is a dual AGN system and double-peaked narrow emission lines could be an effective way of selecting dual AGN candidates. Xu & Komossa (2009) analyzed the line structures and flux ratios of SDSS J1316+1753 in detail, discussing all the possible origins of the double peaks. Furthermore, SDSS J1536+0441 is the only source in which two broad line systems have been found, and it is suggested to be a binary black hole system which is separated by 0.1 pc with an orbital period of 100 yr (Boroson & Lauer 2009). However, it is also the most controversial case, which brings about a great deal of debate (Chornock et al. 2009, 2010; Wrobel & laor 2009; Decarli et al. 2009; Lauer & Boroson 2009; Tang & Grindlay 2009; Gaskell 2010; Dotti & Ruszkowski 2010; Bondi & Pérez-Torres 2010).

The peculiar emission line spectrum of SDSS J1425+3231 was noticed in the course of searching for dual AGN candidates in the SDSS QSO sample. Although SDSS J1425+3231 shows all its strong narrow emission lines to be double-peaked, it is hard to draw conclusions on the structures of the weak emission lines due to the signal-to-noise ratio (S/N). We analyze the spectra of SDSS J1425+3231 in Section 2. The black hole mass is estimated in Section 3. The possible origins of the double-peaked line profiles of this source are discussed in Section 4. The results are summarized in Section 5. Throughout this paper, a cosmology with $H_0 = 70 \, \mathrm{km \, s^{-1} \, Mpc^{-1}}$, $\Omega_M = 0.3$, and $\Omega_\Lambda = 0.7$ is adopted.

2 DATA ANALYSIS

SDSS J1425+3231 is a broad line QSO with an SDSS pipeline-calculated redshift of $z = 0.478$, and all its strong narrow emission lines show double-peaked profiles. In this section, we describe the procedure of spectral fitting. The steps of our analysis are as follows: (1) the spectrum is corrected for foreground Galactic extinction and shifted to the rest-frame by using $z = 0.478$; (2) the continuum of the spectrum is modeled by three components (Hu et al. 2008) and subtracted. The aim is to separate the relative contributions of the continuum and emission line spectrum; (3) multiple Gaussian components are used to fit the emission lines. Steps (2) and (3) are described in more detail below.

2.1 Continuum Decomposition

The continuum is modeled as

$$F_\lambda = F_\lambda^{\mathrm{PL}}(F_{5100}, \alpha) + F_\lambda^{\mathrm{BaC}}(F_{\mathrm{BE}}, \tau_{\mathrm{BE}}) + F_\lambda^{\mathrm{Fe}}(F_{\mathrm{Fe}}, \mathrm{FWHM}_{\mathrm{Fe}}, V_{\mathrm{Fe}}), \qquad (1)$$

where $F_\lambda^{\mathrm{PL}} = F_{5100}(\frac{\lambda}{5100})^\alpha$ is a featureless power law, F_{5100} is the flux at 5100 Å and α is the spectral index. The second and third terms represent the Balmer continuum and Fe emission, respectively.

For wavelengths shortward of the Balmer edge $\lambda < \lambda_{\mathrm{BE}} = 3646$ Å, the Balmer continuum can be expressed as

$$F_\lambda^{\mathrm{BaC}} = F_{\mathrm{BE}} B_\lambda(T_{\mathrm{e}})(1 - \mathrm{e}^{-\tau_\lambda})$$

(Grandi 1982; Dietrich et al. 2002). F_{BE} is a normalization coefficient for the flux at λ_{BE}, $B_\lambda(T_{\mathrm{e}})$ is the Planck function at an electron temperature T_{e}, $\tau_\lambda = \tau_{\mathrm{BE}}(\frac{\lambda}{\lambda_{\mathrm{BE}}})$ is the optical depth at wavelength λ, and τ_{BE} is the optical depth at the Balmer edge. T_{e} is assumed to be $T_{\mathrm{e}} = 15\,000$ K. The two free parameters in the Balmer continuum are F_{BE} and τ_{BE}. At $\lambda > \lambda_{\mathrm{BE}}$, blended higher-order Balmer lines give a smooth rise from $\sim 4\,000$ Å to the Balmer edge (Wills et al. 1985) in the spectrum. However, our fitting windows do not include this region, and in fact our results are not influenced by the higher order Balmer lines.

The optical and ultraviolet Fe II template ($F_\lambda^{\mathrm{I\ Zw\ 1}}$) from NLS1 I Zw 1 is used to subtract the Fe II emission from the spectra (Boroson & Green 1992; Vestergaard & Wilkes 2001). The I Zw 1 template is broadened by convolving it with a Gaussian function G

$$F_\lambda^{\mathrm{Fe}} = F_\lambda^{\mathrm{I\ Zw\ 1}} \times G(F_{\mathrm{conv}}, \mathrm{FWHM}_{\mathrm{conv}}, V_{\mathrm{conv}}), \tag{2}$$

where F_{conv}, $\mathrm{FWHM}_{\mathrm{conv}}$, and V_{conv} are the flux, width and peak velocity shift of the Gaussian function respectively. The parameters of Fe in Equation (1) can be expressed as follows: the flux of the Fe emission, F_{Fe}, is the multiplication of F_{conv} and the flux of the template; the shift of the Fe spectrum is $V_{\mathrm{Fe}} = V_{\mathrm{conv}}$, and the FWHM of the Fe lines is

$$\mathrm{FWHM}_{\mathrm{Fe}} = \sqrt{\mathrm{FWHM}_{\mathrm{I\ Zw\ 1}}^2 + \mathrm{FWHM}_{\mathrm{conv}}^2}.$$

In total, there are seven parameters in the continuum model; they are fitted by minimizing χ^2. The fitting windows include: 2470–2625, 2675–2755, 2855–3010, 3625–3645, 4170–4260, 4430–4650, 5080–5550, and 6050–6200 Å. These windows are free of strong contaminant lines.

Figure 1 shows the result of the continuum decomposition. The Galactic extinction and redshift corrected spectrum are shown in the top panel. The spectrum in the fitting window is plotted in green. The three components of the continuum are shown in blue. The best fit model is shown in red. The middle panel shows the residual spectrum, namely the pure emission line spectrum. We will analyze it in the next step. In the bottom panel, we subtract the power law and the Balmer continuum, and zoom into the Fe-only spectrum in the wavelength range 4100–5600 Å. The Fe model is shown in red.

2.2 Emission Line Fitting

We measured the Hβ and [O III] $\lambda\lambda4959, 5007$ emission lines from the emission line spectrum. Since the narrow lines of this object are double-peaked, two sets of three Gaussian components are used to model [O III] $\lambda4959$ and 5007. One is for the blue component, one for the red component, and one extra Gaussian component is for the underlying broad wing. Fit parameters of all the three Gaussians are the central wavelength, σ and flux. Each [O III] $\lambda4959$ component is forced to have the same centroid and width as the corresponding [O III] $\lambda5007$. In Figure 2, the blue and red components are shown in blue and red respectively. The orange is the underlying wing. The best fit model is shown in green. The three-Gaussian parameterization describes the observed [O III] $\lambda\lambda4959, 5007$ lines very well. The blue and red components are separated by $\sim 500\,\mathrm{km\ s}^{-1}$ in velocity space, and the σ of the blue component is $417\,\mathrm{km\ s}^{-1}$, about 2.2 times broader than the red component. The broad wing (orange) peaks at roughly the same position as that of the blue component. The σ of

the wing is $628 \, \text{km s}^{-1}$. We use four-Gaussian components to model the asymmetric profile of the Hβ emission, two for the blue and red narrow peaks; they are forced to have the same width as the corresponding [O III] λ5007; see the blue and red Gaussians in Figure 2. Different from the fit of [O III], we do not fit a wing to the narrow Hβ component since on the one hand, comparing with the broad Hβ, the strength of the wing can be neglected; on the other hand, the resolution of the SDSS spectrum is not high enough to separate such a weak component from the broad Hβ. The broad Hβ sections are fitted with the other two Gaussian components; see the pink lines. The fitting parameters of each Gaussian component are shown in Table 1.

Table 1 Emission Line Properties of SDSS J1425+3231

Property	Hβ 4861.33	[O III] 4958.91	[O III] 5006.84
Blue system			
Line center (Å)	4861.77±0.51	4957.59±0.08	5005.51±0.08
FWHM (km s^{-1})	417.17±17.77	417.17±17.77	417.17±17.77
Luminosity[a]	44.51±9.88	110.98±11.40	322.76±24.22
Red system			
Line center (Å)	4867.97±0.19	4965.64±0.04	5013.64±0.04
FWHM (km s^{-1})	188.21±5.60	188.21±5.60	188.21±5.60
Luminosity[a]	34.33±4.48	70.31±4.44	212.61±7.59
Wing			
Line center (Å)	–	4957.78±0.31	5005.70±0.31
FWHM (km s^{-1})	–	1281.42±58.31	1281.42±58.31
Luminosity[a]	–	150.33±16.83	419.44±27.07
Broad system			
Line center (Å)	4862.09±0.28	–	–
FWHM (km s^{-1})	1545.02±82.42	–	–
Luminosity[a]	520.66±38.74	–	–
Very broad system[b]			
Line center (Å)	4861.08±0.96	–	–
FWHM (km s^{-1})	4463.45±268.77	–	–
Luminosity[a]	629.68±38.88	–	–

[a] In units of $10^{40} \, \text{erg s}^{-1}$.
[b] Note only the Hβ appears to need the very broad component.

3 MASS OF THE CENTRAL BLACK HOLE

In this section, we use three different methods to estimate the mass of the central black hole.

The first method we used is based on the virial theorem and the $R_{\text{BLR}} - L_{5100}$ relation which is calibrated with the reverberation mapping data. The broad line region (BLR) radius R_{BLR} is estimated from the continuum luminosity at 5100 Å ($L_{5100} = 1.6 \times 10^{40} \, \text{erg s}^{-1} \, \text{Å}^{-1}$) using the $R_{\text{BLR}} - L_{5100}$ relation given by Bentz et al. (2006), then the black hole mass is estimated from $M_{\text{BH}} = f \frac{R_{\text{BLR}} \Delta V^2}{G}$, where f is the scaling factor which is introduced to characterize the unclear kinematics and geometries of the BLRs. Actually, the value of f changes with the shape of the line in use, and $f = 3.85$ is a mean value suggested by Collin et al. (2006). $\Delta V = 1325 \, \text{km s}^{-1}$ is the second moment of the BLR Hβ profile, which is reconstructed from the two pink components in Figure 2. This method gives a value of $8.5 \times 10^7 \, M_\odot$.

The $M_{\text{BH}} - L_{5100}$ relation (see eq. (9) of Peterson et al. 2004) predicts a mass of $3.50 \times 10^8 M_\odot$. We also use the velocity dispersion of gas in the NLR, namely σ of [O III]λ 5007, as a surrogate of the galaxy stellar velocity dispersion σ_* (Nelson 2000), to estimate the central black hole mass based
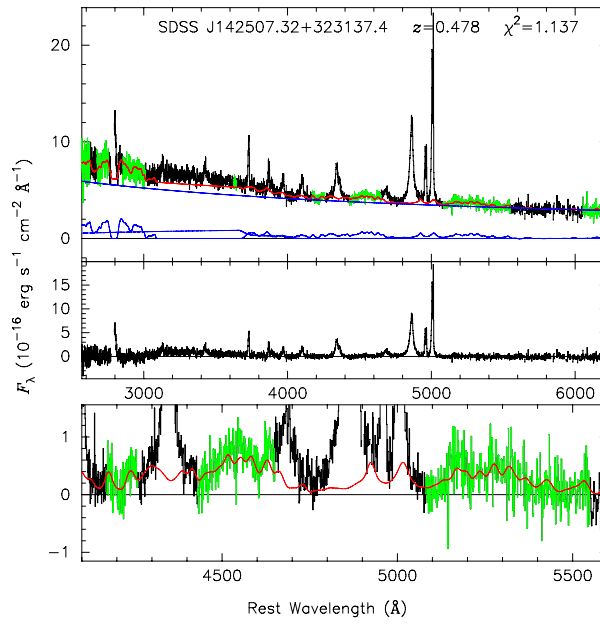
Fig. 1 SDSS spectrum of SDSS J1425+3231 plotted as observed flux versus rest wavelength. The top panel shows the Galactic extinction and redshift corrected spectrum. The spectrum in the fitting window is plotted in green. The three components of the continuum are shown in blue while the best fit model is shown in red. The middle panel shows the residual spectrum, namely the pure emission line spectrum. The bottom panel shows the spectrum after subtracting the power law and the Balmer continuum in the wavelength range 4100–5600 Å. The Fe model is shown in red. The flux density F_λ is given in units of 10^{-17} erg s^{-1} cm^{-2} Å^{-1}.
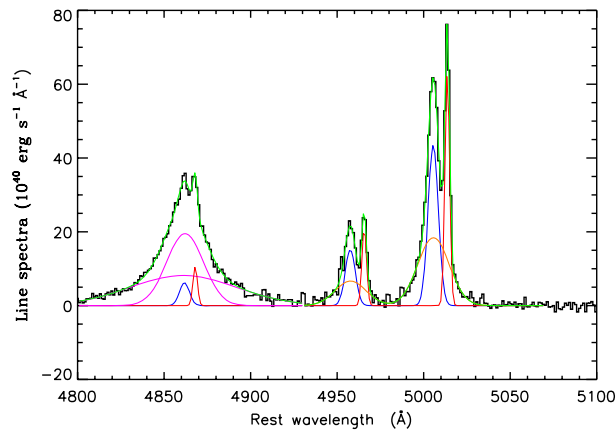
Fig. 2 Emission line fitting of SDSS J1425+3231. For [O III] $\lambda\lambda4959$, 5007 emission lines, three Gaussian components are used. The blue and red Gaussian components represent the two narrow line peaks, and the orange one is the underlying wing. The broad Hβ emission is fitted with four Gaussian components, two for the double-peaked narrow line (red and blue) and another two for the broad line (the two pink components). The best fit model is shown in green.

on the famous $M_{\rm BH} - \sigma_*$ relation which is in the form of $\log(M_{\rm BH}/M_\odot) = 8.13 + 4.02\log(\sigma_*/200)$ (Tremaine et al. 2002). The blue component gives a mass of $8.33 \times 10^7 M_\odot$ with $\sigma = 177.40\,{\rm km\,s^{-1}}$ while the red component indicates a mass of $3.42 \times 10^6 M_\odot$ with $\sigma = 80.18\,{\rm km\,s^{-1}}$.

4 DISCUSSION

4.1 Superposition of Two Objects

The possibility of a superposition in this case is very unlikely for two reasons. First, the red component of [O III]λ 5007 has a luminosity of 3.2×10^{42} erg s^{-1}, while the σ of this line indicates a black hole mass of $3.42 \times 10^6 M_\odot$. If this component comes from a background AGN, its accretion rate should be extremely super-Eddington, which is hard to explain (see Sect. 4.3 for the explanation under the dual AGN scenario). Second, Dotti & Ruszkowski (2010) examined the superposition model of double-peaked emission line AGNs based on galaxy clusters from the Millennium Run, finding that the fraction of superimposed galaxy pairs peaks at about $z = 0.2$ and decreases rapidly from $z = 0.3$. Considering the redshift of SDSS J1425+3231, ~ 0.478, the possibility of superposition should be very low.

4.2 NLR Kinematics

Another possible explanation for the double-peaked narrow emission could be special NLR geometries such as biconical outflows or disk-like NLRs. In such a hypothesis, there is only one AGN to illuminate the NLR gas which is moving toward and away from us, forming the blue and red components in the observed narrow lines.

Certain nearby Seyfert and star forming galaxies are known to have biconic outflow induced double-peaked emission lines. The examples are found not only from the spatially resolved spectra which are taken along the minor axis of the galaxy (e.g. Cecil 1988; Cecil et al. 1990; Veilleux et al. 1994, 2001; Colbert et al. 1996) but also from the spectrum of the whole galaxy (e.g. Duric & Seaquist 1988; Axon et al. 1998). In the scenario of biconic outflows, we would expect that the blue and red components have the same velocity dispersion since they are illuminated by the same AGN. However, in SDSS J1425+3231, the blue component is three times broader than the red component, which conflicts with the outflow model. On the other hand, the outflow studies find that the NLRs are stratified strongly in ionization and velocity so that high-ionization lines, such as [O III], originated near the AGN with higher velocity and low-ionization lines, but other lines, such as Hβ and [O II], originated further from the AGN with lower velocity (e.g., Komossa et al. 2008). In SDSS J1425+3231, we find that [O III] and Hβ are consistent in their velocity offsets within error bars, and apparently no ionization stratification is observed as expected in AGN driven outflows. In addition, the [O III]λ5007 luminosity is 4.3×10^{42} erg s^{-1} for the blue system and 2.8×10^{42} erg s^{-1} for the red system. These are typical values for the emission from all the NLRs of bright Seyfert galaxies and quasars, but it is hard to imagine that all the NLRs are outflowing.

The observed double-peaked narrow emission lines can be accounted for in a disk-like NLR model. The rotating disk model predicts that the blue and red components have similar widths, which conflicts with the current data. Furthermore, the red and blue components are expected to be (almost) equally shifted with respect to the true cosmological galaxy redshift in this scenario. We are lacking host galaxy information since it is overpowered by the central AGN. However, under the disk-like NLR model, the broad line should be at the redshift of the galaxy, in between the blue and red components, and not so close to the the blue component as we have seen from the data.

4.3 A Dual AGN System

The final picture we want to suggest for SDSS J1425+3231 is that this is a dual AGN system. The primary black hole in this system has a mass of $\sim 10^8\,M_\odot$. The observed blue narrow component in

[O III]$\lambda\lambda$4959, 5007, the broad Hβ component and the wing of [O III]$\lambda\lambda$4959, 5007 are generated in its NLR, BLR and the region in between (this region is usually referred as an intermediate line region in literatures) respectively. The consistency between the black hole masses estimated from the broad Hβ component and the σ of the blue component supports this idea. We have not observed the broad emission lines from the BLR of the secondary black hole ($\sim 10^6 \, M_\odot$); the possible reasons for this include: (1) the S/N of SDSS spectra is not high enough for us to separate the broad emission line of the secondary black hole from the primary one; (2) the secondary black hole is a type 2 AGN in which the BLR is obscured by the dusty torus.

The only issue about the dual AGN system is that, for the secondary black hole, comparing with the [O III]λ 5007 luminosity, a mass of $10^6 \, M_\odot$ is a bit low. This indicates the secondary black hole is accreting in a super Eddington regime. At first sight, this conflicts with the normally accepted accretion theory. However, we should note that in the dual AGN case, the separation between the two black holes is on the kpc scale, so the NLR gas of the secondary black hole can be affected by the primary black hole, namely because the primary black hole can illuminate the NLR of the secondary black hole.

5 CONCLUSIONS

Type 1 QSO SDSS J1425+3231 has double-peaked narrow emission lines. In this paper, we analyze the SDSS spectrum of this object, discussing the origins of its double-peaked line structure. We argue against the possibility of superposition of two objects, biconic outflows or disk-like NLRs, and we propose that this is a dual AGN system.

In this system, since the observed broad lines are from the primary black hole, it has a mass of $\sim 10^8 \, M_\odot$. The secondary black hole is much smaller; its mass is on the order of $10^6 \, M_\odot$. The secondary black hole could be a type 2 AGN whose BLR is obscured, or we might have failed to separate the broad emission line of the secondary black hole from that of the primary black hole due to the resolution of the SDSS spectra.

In future observations, a high spatial resolution two-dimensional optical spectrum and imaging in the optical, radio and X-ray would help us figure out whether SDSS J1425+3231 contains dual AGNs. Moreover, the ultimate confirmation or rejection of the dual AGN interpretation, which predicts variations in the line profiles, will come from multi-epoch spectroscopic monitoring.

References

Axon, D. J., et al. 1998, ApJ, 496, L75

Bondi, M., & Pérez-Torres, M-A. 2010, ApJ, 714, L271

Bentz, M. C., et al. 2006, ApJ, 644, 133

Boroson, T. A., & Green, R. F. 1992, ApJS, 80, 109

Boroson, T. A., & Lauer, T. R. 2009, Nature, 458, 53

Cecil, G. 1988, ApJ, 329, 38

Cecil, G., Bland, J., & Tully, R. B. 1990, ApJ, 355, 70

Chornock, R., et al. 2009, The Astronomer's Telegram, 1955, 1

Chornock, R., et al. 2010, ApJ, 709, L39

Colbert, E. J. M., et al. 1996, ApJS, 105, 75

Collin, S., Kawaguchi, T., Peterson, B. M., & Vestergaard, M. 2006, A&A, 456, 75

Colpi, M., & Dotti, M. 2009, arXiv:0906.4339

Comerford, J., et al. 2009a, ApJ, 698, 956

Comerford, J., et al. 2009b, ApJ, 702, L82

Decarli, R., et al. 2009, ApJ, 703, L76

Dietrich, M., et al. 2002, ApJ, 564, 581

Dotti, M., & Ruszkowski, M. 2010, ApJ, 713, L37

Dotti, M., et al. 2009, MNRAS, 398, L73

Duric, N., & Seaquist, E. R. 1988, ApJ, 326, 574

Gaskell, C. M. 2010, Nature, 463, E1

Gerke, B., et al. 2007, ApJ, 660, L23

Grandi, S. A. 1982, ApJ, 255, 25

Greene, J. E., & Ho, L. C. 2005, ApJ, 627, 721

Heckman, T. M., Miley, G. K., van Breugel, W. J. M., & Butcher, H. R. 1981, ApJ, 247, 403

Heckman, T. M., Miley, G. K., & Green, R. F. 1984, ApJ, 281, 525

Hu, C., et al. 2008. ApJ, 687, 78

Komossa, S. 2006, Mem. Soc. Astron. Ital., 77, 733

Komossa, S., et al. 2003, ApJ, 582, L15

Komossa, S., et al. 2008, ApJ, 680, 926

Lauer, T. R., & Boroson, T. A. 2009, ApJ, 703, 930

Liu, X., Greene, J. E., Shen, Y., & Strauss, M. A. 2010, ApJ, 715, L30

Morganti, R., Emonts, B., & Osterloo, T. 2009, A&A, 496, L9

Nelson, C. H. 2000, ApJ, 544, L91

Peterson, B. M., et al. 2004, ApJ, 613, 682

Rodriguez, C., et al. 2006, ApJ, 646, 49

Rodriguez, C., et al. 2009, ApJ, 697, 37

Tang, S., & Grindlay, J. 2009, ApJ, 704, 1189

Tremaine, S., et al. 2002, ApJ, 574, 740

Veilleux, S., Shopbell, P. L., & Miller, S. T. 2001, AJ, 121, 198

Veilleux, S., et al. 1994, ApJ, 433, 48

Vestergaard, M., & Wilkes, B. J. 2001, ApJS, 134, 1

Wang, J., Chen, Y., Hu, C., Mao, W., Zhang, S., & Bian, W. 2009, ApJ, 705, L76

Wills, B. J., Netzer, H., & Wills, D. 1985, ApJ, 288, 94

Wrobel, J. M., & Laor, A. 2009, ApJ, 699, L22

Xu, D., & Komossa, S. 2009, ApJ, 705, L20

Zhou, H., Wang, T., Zhang, X., Dong, X., & Li, C. 2004, ApJ, 604, L33